Int. J. Heat Mass Transfer. Vol. 15, pp. 2611–2631. Pergamon Press 1972. Printed in Great Britain

EXPERIMENTAL STUDY OF EFFECT OF WETTING ON TURBULENT FLOW OF MERCURY IN ANNULI*

P. J. HLAVAC, B. G. NIMMO and O. E. DWYER

Department of Applied Science, Brookhaven National Laboratory, Upton, New York 11973, U.S.A.

(*Received* 15 *November* 1971 *and in revised form* 5 *April* 1972)

Abstract—A basic experimental study of the fluid dynamics and heat transfer characteristics of mercury, in fully developed turbulent flow through annuli, was carried out. The main purposes of the study were, first, to get comparisons between local ε_H and ε_M values, and second, to determine the effects of wetting on both the fluid dynamics and heat transfer. This paper presents the results of the fluid dynamics portion of the study.

Experiments were conducted where the mercury either did not wet at all, or did thoroughly wet, the channel walls. The effects of wetting were found to be appreciable. When both annulus walls were unwetted, the velocity profiles were quite similar to those reported in the past for ordinary fluids. When the inner wall (only) was wetted, the radius of maximum velocity moved considerably outward (i.e. toward r_2) from what it was when both walls were unwetted; and when both walls were wetted, the radius of maximum velocity also moved outward, but not as far as that for the situation where only the inner wall was wetted. These differences in flow behavior are reflected in the u^+ vs. ln y^+ relationships and in the ε_M profiles.

Wetting was found to have a large influence on the u^+ vs. ln y^+ relationship for the inner portion of an annulus. The eddy diffusivities of momentum transfer were correlated only moderately well by modified forms of the Kays–Leung [6] and Eifler [13] correlations. It is shown that the ratio of the maximum value of ε_M in the inner portion of an annulus to that in the outer portion is an explicit function of the radius ratio and is independent of Reynolds number.

NOMENCLATURE

B, coefficient in equation $\beta = BRe^{0.1}$, refers to equation (18) [dimensionless];

B_1, B_2, values of B for inner and outer portions, respectively, of annulus, [dimensionless];

D_e $2(r_2 - r_1)$, equivalent diameter of annulus [ft];

g_c, conversion factor $\left[\frac{\text{lb}_m}{\text{lb}_f}\frac{\text{ft}}{\text{h}^2}\right]$;

inner portion, that portion of annulus between r_1 and r_m;

L, length of annular channel between traversing stations [ft];

outer portion, that portion of annulus between r_m and r_2;

p, static pressure [lb_f/ft^2];

r, radial distance [ft];

r_m, radius of maximum time-average velocity [ft];

r_1, r_2, inner and outer radii, respectively, of annulus [ft];

r_2^+, $(r_2/\nu)\sqrt{(\tau_{w2}g_c)/\rho}$, dimensionless outer radius of annulus;

Re, $D_e v_a \rho/\mu$, Reynolds number for annulus [dimensionless];

$\bar{s}$, r_m/r_2, [dimensionless];

t_1, t_2, constants in equation (18) for inner and outer portions, respectively, of annulus [dimensionless];

u^*, $\sqrt{(\tau_w g_c)/\rho}$ = friction velocity for flow in circular tubes (ft/h);

* This work was performed under the auspices of the U.S. Atomic Energy Commission.

u_1^*, $\sqrt{(\tau_{w1} g_c)/\rho}$ = friction velocity for flow in inner portion of annulus [ft/h];

u_2^*, $\sqrt{(\tau_{w2} g_c)/\rho}$ = friction velocity for flow in outer portion of annulus [ft/h];

u^+, v/u^*, dimensionless velocity parameter for flow in circular tubes;

u_1^+, v/u_1^*, dimensionless velocity parameter for fluid flowing in inner portion of annulus;

u_2^+, v/u_2^*, dimensionless velocity parameter for fluid flowing in outer portion of annulus;

v, local time-mean velocity in annular channel at radial distance r [ft/h];

v_a, average value of v across entire annulus [ft/h];

v_{max} maximum value of v [ft/h];

y, distance measured normal to wall, in flow through circular tubes [ft];

y_1, y_2, distances measured normal to inner and outer walls, respectively, in flow through annuli [ft];

y^+, $\dfrac{y\sqrt{(\tau_w g_c)/\rho}}{\nu}$ = dimensionless distance from the wall, with reference to flow in circular tubes;

y_1^+, $\dfrac{y_1\sqrt{(\tau_{w1} g_c)/\rho}}{\nu}$ = dimensionless distance from the inner wall of nucleus;

y_2^+, $\dfrac{y_2\sqrt{(\tau_{w2} g_c)/\rho}}{\nu}$ = dimensionless distance from outer wall of annulus;

z_1, z_2, geometrical functions, defined by equation (21), for inner and outer portions, respectively, of annulus [dimensionless];

α reciprocal coefficient in equation (11) [dimensionless];

β, coefficient in equation (18) [dimensionless];

ε_H, eddy diffusivity of heat transfer at radial distance r [ft^2/h];

ε_M, eddy diffusivity of momentum transfer at radial distance r [ft^2/h];

$\varepsilon_{M1}, \varepsilon_{M2}$, same as ε_M, except for inner and outer portions, respectively, of annulus;

$[\varepsilon_M]_{min}$, value of ε_M where the ε_M profile curve goes through a minimum;

$[\varepsilon_{M1}]_{max.}$, $[\varepsilon_{M2}]_{max.}$ maximum values of ε_{M1} and ε_{M2}, respectively;

ε_M^+, general symbol for either ε_{M1}^+ or ε_{M2}^+, dimensionless eddy diffusivity;

ε_{M1}^+, $\dfrac{\varepsilon_{M1}}{u_1^*(r_m - r_1)}$ = dimensionless eddy diffusivity for inner portion of annulus;

ε_{M2}^+, $\dfrac{\varepsilon_{M2}}{u_2^*(r_2 - r_m)}$ = dimensionless eddy diffusivity for outer portion of annulus;

η_1, $(r_m - r)/(r_m - r_1)$ = radial coordinate, referred to inner wall [dimensionless];

η_2, $(r_m - r)/(r_m - r_2)$ = radial coordinate, referred to outer wall [dimensionless];

μ, viscosity [lb$_m$/hft];

ν, μ/ρ, kinematic viscosity [ft^2/h];

ρ, density [lb$_m$/ft^3];

τ, shear stress at radial distance r [lb$_f$/ft^2];

τ_1, $\left(\dfrac{\Delta p}{\Delta L}\right)\dfrac{(r_m^2 - r^2)}{2r}$,

τ_2, shear stress at radial distance r in inner portion of annulus $[lb_f/ft^2]$; $\left(\frac{\Delta p}{\Delta L}\right)\frac{(r^2 - r_m^2)}{2r}$,

τ_{w1}, shear stress at radial distance r in outer portion of annulus $[lb_f/ft^2]$; $\left(\frac{\Delta p}{\Delta L}\right)\frac{(r_m^2 - r_1^2)}{2r_1}$,

τ_{w2}, shear stress at inner wall of annulus $[lb_f/ft^2]$; $\left(\frac{\Delta p}{\Delta L}\right)\frac{(r_2^2 - r_m^2)}{2r_2}$,

shear stress at outer wall of annulus $[lb_f/ft^2]$.

1. INTRODUCTION

A BASIC experimental study of heat transfer to mercury flowing turbulently in smooth annuli was carried out. Heat was transferred from the inner wall only, the flux was uniform in all directions, and the outer wall was adiabatic. Data, taken only under fully developed flow and heat transfer, consisted of the following measurements: axial pressure drop, time-mean-velocity profiles, time-mean-temperature profiles, time-mean heating surface temperatures, and inlet and outlet bulk temperatures. The measurements were made with both walls wetted by the mercury, with both walls unwetted, and with the inner wall wetted and the outer wall unwetted.

The purpose of the present paper is to present the fluid dynamic results. These include velocity profiles, radii of maximum velocity, and eddy diffusivities of momentum transfer. Two additional papers will be published later—one [1] on the eddy diffusivity of heat transfer and its relations to its momentum counterpart, and the other [2] on the measurement and prediction of heat transfer coefficients. In all three papers, attention will be focused on the effects of wetting vs. nonwetting on the various dependent parameters.

2. EXPERIMENTAL EQUIPMENT

2.1 *Test loop*

The experiments were carried out in a simple recirculating loop built of stainless-steel pipe. The mercury flowed vertically downward through the test section, whence it flowed through a horizontal section containing an orifice flowmeter. This flowmeter had interchangeable, rounded, stainless-steel orifices that had been previously calibrated with water. From the flowmeter, the mercury passed consecutively through a water-cooled heat exchanger, a surge tank, and a pump. The loop operated in the temperature range 110–125°F.

The mercury used was the chemically pure, distilled grade; and the cover gas in the surge and dump tanks was pure nitrogen. A porous stainless-steel filter was located in a bypass line around the pump to remove any particulate matter in the mercury. At certain intervals, the mercury was drained to the dump tank, from where it was later recharged into the loop (by gas pressure) through a dip leg, thereby trapping any floating oxides, or other particulate material, in the dump tank. It was important to maintain very clean mercury in the loop to prevent plugging of the miniature pitot tubes used for measuring the velocity profiles.

2.2 *Test sections*

Three different test sections were used. They had r_2/r_1 ratios of 2·09, 2·78 and 4·00. The first and third were of the same basic design; the second was slightly different, as explained below. A schematic drawing (representing either 2·09 or 4·00) is shown in Fig. 1, giving the locations of the traversing stations and certain pertinent information. Basically, a test section consisted of a long stainless-steel pipe in which an electrical rod heater was concentrically positioned. The mercury entered the test section at the top through two 2-in. pipes, 180 degrees apart, and left in the same manner at the bottom. The mercury entered the annular channel (from a small, circular plenum chamber) through four

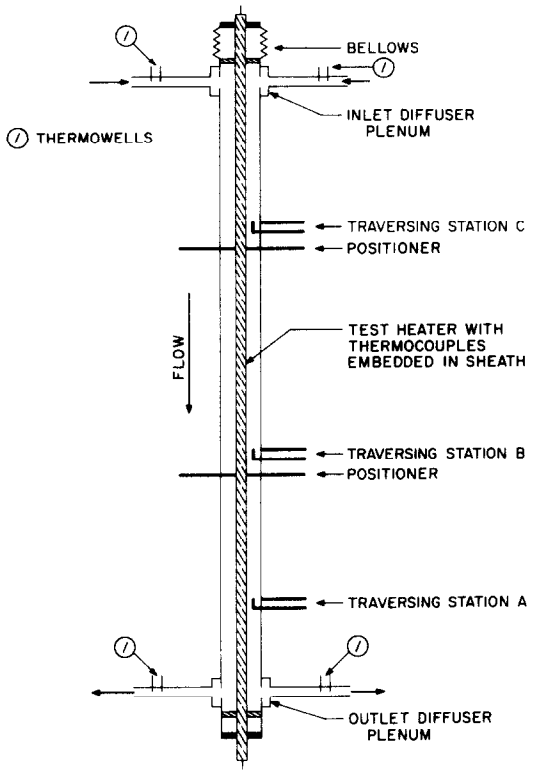

FIG. 1. Schematic drawing of test section. The thermal insulation is not shown, and the drawing is not to scale.

$\frac{5}{8}$ in. dia. holes 90 degrees apart on the circumference of the outer pipe. The mercury left the annular channel at the bottom in the same manner. The purpose of these diffuser plenums was to maximize the length of the test section over which fully developed flow occurred.

Each of the test sections had three traversing stations for measuring the temperature and velocity profiles. These stations were located at certain axial distances from the flow inlet point. These, in terms of equivalent diameters, are given in Table 1. At each traversing station, there were three pressure taps, one temperature probe, and two velocity probes. The paths traversed by the probes were 120 degrees apart on the circumference.

Table 1. Axial locations of the three traversing stations

	No. of equivalent diameters from flow inlet point		
r_2/r_1	Station A	Station B	Station C
2·09	127	95	48
2·78	79	58	39
4·00	88	66	33

In one test section ($r_2/r_1 = 2{\cdot}78$), a so-called positioning station was located ~ 5 equivalent diameters below traversing station C. Its purpose was to keep the heater rod concentric with the pipe. The positioner consisted of three streamlined, stainless steel pins, 120 degrees apart, which could be moved in and out across the flow channels by means of screw mechanisms. The radial location of the tip was read on a vernier scale and believed to be accurate to $\pm 0{\cdot}001$ in. In the two other test sections, there were two positioners of the same design, except they had four pins instead of three. They were located $\sim 1{\cdot}3$ equivalent diameters below traversing stations B and C in one ($r_2/r_1 = 2{\cdot}09$) test section, and $\sim 0{\cdot}9$ in the other ($r_2/r_1 = 4{\cdot}00$).

After fabrication, the inner surface of the test-section pipe was honed, with all station seals assembled, to eliminate any projections or roughness which could perturb the flow pattern. The honing produced a final surface finish having a roughness of 10–12 μin. (r.m.s.).

2.3 *Velocity probes*

These consisted of a 0·027 in. i.d. × 0·043 in. o.d. stainless-steel hypodermic tube centred in a $\frac{1}{8}$ in. dia. stainless-steel rod. The radial position of the sensing tip was read on a micrometer gage to a precision of $\pm 0{\cdot}001$ in. The hypodermic tube extended about $\frac{1}{4}$ in. upstream, beyond the end of the rod, i.e. it was bent 90°. That portion of the rod which entered the flow channel was ground into a streamline shape, presenting a maximum dimension of 0·040 in. to the flowing mercury. The tip of the hypodermic tube was flattened and ground so that the flatter sides faced the channel walls. The flattened tip had outside dimensions of about 0·040 in. × 0·015 in., making it possible to take readings to within

0·008 in. of each wall. It was estimated that the radial position of the center of the sensing tip was measured with an accuracy of ±0·003 in. The outer surface of the probe tip was beveled, by grinding, to produce a knife-edge to the approaching stream. According to the recommendations of Livesey [3], these probes should have given negligible errors resulting from steep velocity gradients.

The velocity pressure heads were measured by means of U-tube mercury manometers.

2.4 *Channel walls*

The rod heaters, which, with the surrounding pipe, formed the annular-shaped channels, were special electrical heaters. Their design and construction will be described in detail in [2]. In the present paper, it is sufficient to describe their outer surfaces. The heaters had 0·110 in. thick copper sheaths, over which a 0·001 in. layer of nickel was electroplated. This was followed by a final 0·0001 in. thick electroplate of chromium, if a nonwetting surface was desired, or by a final 0·0004 in. thick electroplate of copper, if a wetting surface was desired. In the latter case, the copper flash coating was soon dissolved away by the mercury, exposing a completely wetted nickel surface. Before insertion in the test section, each heater was carefully checked for straightness, and straightened if necessary. It was then cleaned with a detergent, thoroughly rinsed with water, rinsed with acetone, wiped dry with pure unspun cotton, and inserted immediately in the test section.

3. EXPERIMENTAL PROCEDURES

The experimental results presented in this paper were obtained under essentially isothermal flow through the test section, i.e. no power on the heater rods.

3.1 *Pressure-drop measurements*

The pressure-drop data were taken across the channel length between traversing stations A and B. Measurements between stations B and C were a few per cent greater, presumably because of the existence of a slight entrance effect in that region. All readings were taken with the velocity and temperature probes backed out until they were adjacent to the outer wall.

There was about 9 ft of vertical distance between station B and the manometer connection. Because of this, it was necessary to maintain the same temperature along this line as that in the test section. This was done by adjusting the temperature of the flowing stream until it equalled that of the mercury in the pressure-tap line.

Temperature readings were taken of: the inlet mercury, the outlet mercury, the mercury along the $\frac{1}{4}$ in. line from station B, and the mercury in the manometer. The flow rate was measured by means of a recording orifice flowmeter, for which an orifice size was selected that would give the greatest accuracy over the flow range covered.

3.2 *Local velocity measurements*

The three static-pressure taps and the sensing tip of the pitot-tube velocity probe (at each traversing station) were, in all cases, at the exact same level. The three static-pressure taps were manifolded together, and a single line led to the low-pressure side of the manometer. Before the pump was turned on, the zero-flow reading on the manometer was determined. If it was not zero, it was sometimes because of gas in the lines but more usually because of particulate matter in the probe sensing tip. The problem was eliminated by back-flushing the lines with clean mercury from a pressurized reservoir. All probes but the one in use were backed out of the flow channel until they were adjacent to the outer wall.

The pump was then turned on, and the desired flow rate established. After waiting a few minutes for the system to reach steady state, at least three readings were taken over an interval of about five minutes, after setting the probe tip at the desired radial position. Valves in the manometer connecting lines were used to damp the manometer fluctuations.

All of the velocity profiles presented in this paper were determined at station A, and usually with only one of the two velocity probes. There was little difference observed between the data taken at station A and those taken at station B, and no difference between those taken on the two probes (120° apart) at station A.

Each velocity profile that was determined was based upon at least three complete traverses with the probe. As shown later, the reproducibility of the data for a given flow rate was quite good. On the average, v_a as calculated from the integrated velocity profile was 2·7 per cent greater than v_a as obtained from the flowmeter readings, for all the runs made with the 2·09 (r_2/r_1) annulus. The corresponding values for the 2·78 and 4·00 annuli were −0·1 per cent and 3·5 per cent respectively. The integral values were used in all the calculations and correlations, because they were the ones that were consistent with the local v (observed) and local ε_M (calculated) values.

4. RESULTS

4.1 *Velocity profiles*

Figure 2 shows a series of time-mean velocity profiles with their data points to illustrate the precision of the data. Figure 3 shows a set of velocity distribution curves that illustrate the effect of change in Reynolds number and the effect of wetting on the shape of the velocity-profile curve. The final velocity profiles obtained in the present study were determined as follows: (1) the original data points (from three to five sets of data) were plotted on a v vs. r plane, for each Reynolds number, (2) smooth curves were then drawn through the points, (3) v vs. Reynolds number cross-plots were then made for many values of r between r_1 and r_2, and (4) final v vs. r curves were then obtained, with Reynolds number as the parameter.

Wetting of a wall by the mercury produces a drag force on the flowing steam that tends to push the radius of maximum velocity farther away from that wall. This causes the profile for the case of inner wall wetted and outer wall unwetted to be the most symmetrical across the channel. The biggest effect of wetting occurs in the inner portion of the annulus, i.e. across the radial distance r_1 to r_m. In Fig. 3, it is seen that this effect was greater than that produced by a four-fold change in the Reynolds number.

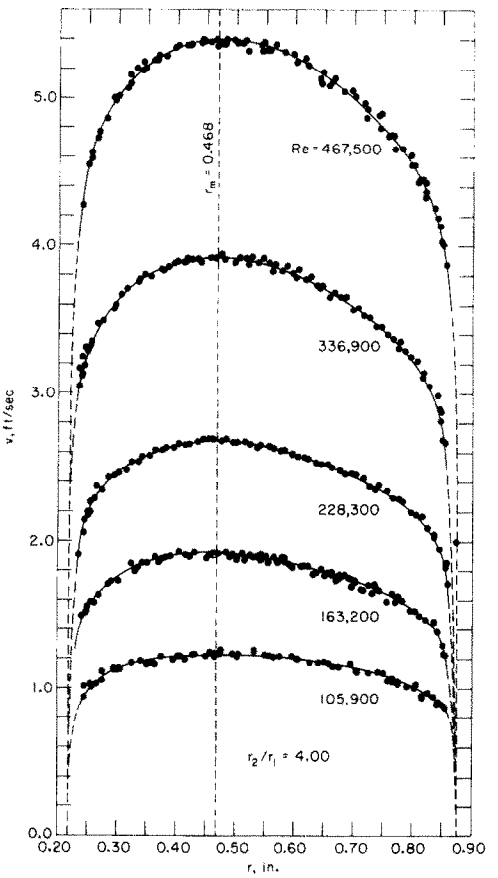

FIG. 2. Typical plot showing time-mean velocity distribution data. They are for the case of both walls unwetted.

The effect of surface wetting and the effect of the physicochemical properties of the wall–liquid interface on fluid dynamic behaviour in channel flow are discussed in a review article by Smolskii and Elperin [4]. Dokuchaev [5] compared velocity profiles for water flowing in glass* (wetted) and Plexiglas (unwetted) tubes.

* Assumed by present authors, not made clear in [4].

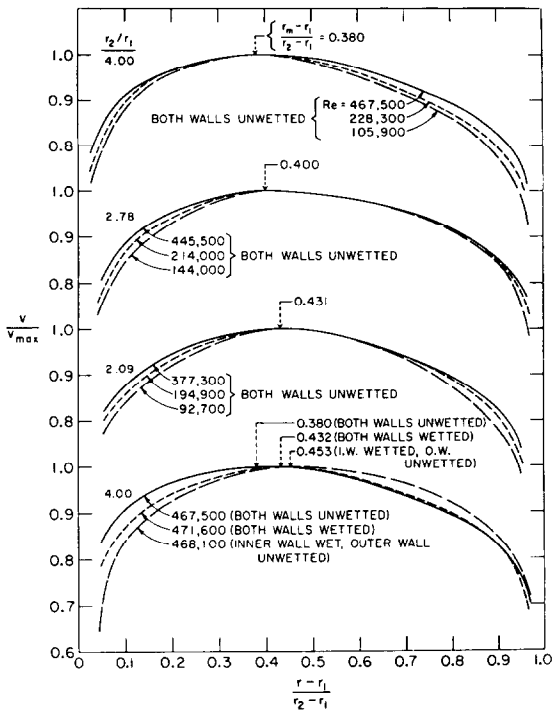

FIG. 3. Measured time-mean velocity distribution curves showing the effects of Reynolds number and wetting.

He observed that the velocity profile near the wall in the "unwetted" case was steeper than that in the "wetted" case. These observations are consistent with those reported here. However, it is generally assumed that degree of wetting has a negligible effect on fluid dynamic behavior, but no results have, to the present authors' knowledge, been reported for wetting mercury systems. The type of wetting one gets with such systems is very different from that associated with ordinary liquids. In the case of nickel wetted by mercury (the wetting system in the present study), for example, there is a bimetallic compound formed at the interface. However, in the case of water wetting nickel, it is simply a surface tension effect, the surface tension of the nickel–water system being much lower than, for example, the air–water system. Thus, the wetting of nickel by mercury is essentially chemical in nature, while that by water is essentially physical. And, it now appears that this difference in physico-chemical characteristics at the liquid–solid interface is reflected in the flow behavior in the liquid, particularly near the wall.

4.2 *Radius of maximum velocity*

The radius of maximum velocity was obtained from the velocity data by plotting $(v' - v)$ vs. r, where v' was arbitrarily taken to be just slightly greater than v_{max}. The radius of maximum velocity was taken as the radius at which the $(v' - v)$ curves (drawn through points) for the inner and outer portions of the annulus intersected.

The experimental results are summarized in Table 2 and Fig. 4, where they are given in terms of the dimensionless ratio $(r_m - r_1)/(r_2 - r_m)$ as a function of the r_1/r_2 ratio. It should be stated that each value of $(r_m - r_1)/(r_2 - r_m)$ in Table 2 and each data-point symbol represents the average of at least four, and generally five, separate v vs. r curves, each at a different Reynolds number. These Reynolds numbers varied over a 4- to 5-fold range, and there was very good agreement on the location of r_m, other conditions remaining the same. Strictly speaking, r_m should have a very slight dependence on the Reynolds number at the higher r_2/r_1 ratios, but for the test conditions of the present study, the dependence is unquestionably insignificant.

Table 2. Radii of maximum velocity, as determined in present study

r_2/r_1	Wetting conditions: Inner wall	Wetting conditions: Outer wall	r_m(in.)	$\frac{r_m-r_1}{r_2-r_m}$
2·09	Wetted	Unwetted	0·632	0·874
	Unwetted	Unwetted	0·616	0·759
2·78	Unwetted	Unwetted	0·428	0·668
4·00	Wetted	Wetted	0·502	0·759
	Wetted	Unwetted	0·516	0·828
	Unwetted	Unwetted	0·468	0·612

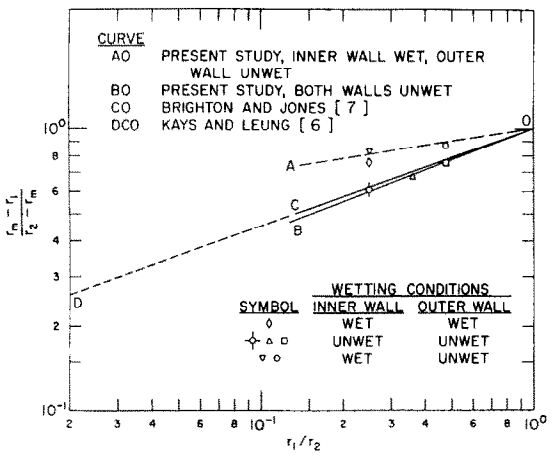

FIG. 4. Summary of present results and generally recommended correlations, relative to the determination of radius of maximum velocity for turbulent flow in smooth annuli.

An interesting finding in the present study was the effect of degree of wetting on the location of r_m. It was large and very reproducible. The results of the present study are compared, in Fig. 4, with the line $\overline{DCO}$, which is apparently the best correlation for expressing r_m as a function of r_1/r_2, for fully developed turbulent flow of ordinary fluids in annuli. This line represents the empirical equation

$$\frac{r_m - r_1}{r_2 - r_m} = (r_1/r_2)^{0.343} \qquad (1)$$

proposed by Kays and Leung [6]. It is based on experimental results obtained (on air and water) in three different investigations. The $\overline{CO}$ portion of line $\overline{DCO}$ was later confirmed by experimental results obtained by Brighton and Jones [7] on air.

It is seen that the mercury results for the case of both walls unwetted (line $\overline{BO}$) fell very slightly *below* line $\overline{DCO}$, while the results with the inner wall wetted and the outer wall unwetted fell considerably *above* line $\overline{DCO}$. The results for both walls wetted also fell considerably above line $\overline{DCO}$, but not as much as those for the case of a wetted inner wall and an unwetted outer wall. These effects of surface wetting are reflected in the ε_M vs. r profiles presented later, because of the sensitive dependence of the axial shear stress profile on the value of r_m.

It is apparent that the fluid dyanmics of mercury flowing in an annulus with both walls unwetted is not appreciably different from that of ordinary fluids. The layer of fluid molecules adjacent to the wall is stationary in the two cases, and the degree of slippage of the liquid "layers" near the wall is not appreciably different in the two cases either. On the other hand, when the mercury wets the wall, there appears to be an added drag on the liquid at the wall, which propagates out into the flowing stream. This would account for the relative positions of the symbols in Fig. 4 for $r_1/r_2 = 0{\cdot}25$. When only the inner wall is wetted, r_m is considerably larger than when both walls are unwetted. And, when both walls are wetted, r_m tends to approach that for both walls unwetted, but, because of the large difference in the cross-sectional areas between r_1 and r_m on the one hand and r_m and r_2 on the other, r_m for both walls wetted is nearer that for the case of the inner wall wetted and the outer wall unwetted. It is pointed out that each symbol represents the average value of r_m from 15 to 20 sets of original data.

For the case of the inner wall wetted and the outer wall unwetted, the exponent in equation (1) should be changed to 0·16, according to the line $\overline{AO}$. For the case of both walls unwetted, it should be changed to 0·37, according to the line $\overline{BO}$.

4.3 u^+ *vs.* $ln\, y^+$ *correlations*

All of the velocity data were reduced and plotted on law-of-the-wall u^+ vs. $\ln y^+$ planes. The velocity measurements taken in the inner portions of the annuli (i.e. between r_1 and r_m) were plotted on u_1^+ vs. $\ln y_1^+$ planes, while those taken in the outer portions (i.e. between r_m and r_2) were plotted on u_2^+ vs. $\ln y_2^+$ planes. A typical plot is shown in Fig. 5. There was no significant difference between the scatter of

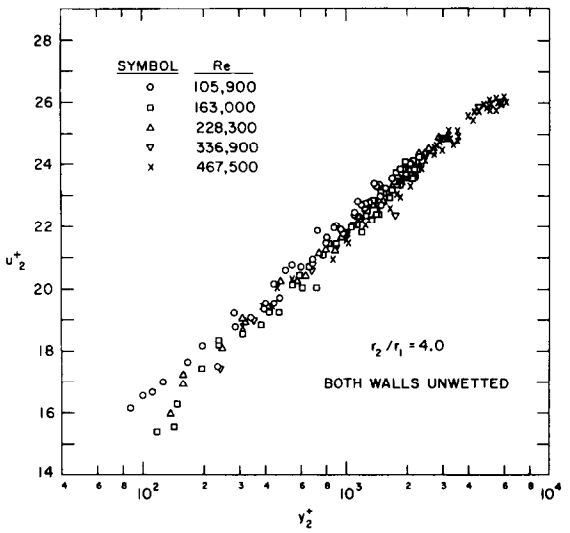

FIG. 5. Typical experimental data, showing velocity distribution in *outer* portion (i.e. between r_m and r_2) of concentric annulus for fully developed, turbulent flow of mercury, and for unwetted walls.

inner-portion data points and that of outer-portion points; and there was no significant effect of wetting on data scatter.

The data points in 9 of the 12 u^+ vs. ln y^+ plots unmistakably obeyed the logarithmic law and gave straight lines, as in Fig. 5. The three plots that did not give straight lines were the u_1^+ vs. ln y_1^+ plots for the annulus with the largest r_2/r_1 value (4·00). This information, summarized in Table 3, is discussed in more detail later.

4.3.1 *Dependency on Reynolds number.* The data points in Fig. 5 show a very slight dependency of u_2^+ on the Reynolds number, the higher Reynolds numbers tending to give lower values of u_2^+. In general, this was found to be true for u_2^+ vs. ln y_2^+ plots for the larger r_2/r_1 ratios. In these cases, the opposite was generally found to be true for u_1^+ vs. ln y_1^+. This agrees with the finding of Quarmby [8], who varied the Reynolds number over a 4- to 6-fold range in annuli having r_2/r_1 ratios of 2·88, 5·62 and 9·37. Brighton and Jones [7] varied the Reynolds number 3- to 4-fold, but their results were, for the most part, inconclusive on this point. These investigators obtained their results with air.

The effects of Reynolds number on u_1^+ and u_2^+, as observed in the present study, are summarized qualitatively in Table 4. There was no observable effect on the data from the annulus having the smallest r_2/r_1 ratio (2·09). These results would seem to indicate that there should be more of a Reynolds number effect for flow in pipes than for flow between parallel plates.

The u^+ vs. ln y^+ plot that showed the greatest scatter was that for the case of $r_2/r_1 = 4·0$, inner wall wetted, outer wall unwetted, and for the outer portion of the annulus. However, when the data points for the five different Reynolds numbers were plotted separately, they showed very little scatter, and each set gave a good straight line. The results are shown in Table 5, in terms of the correlating equations.

Table 3. Summary of u^+ *vs. ln* y^+ *results*

			Logarithmic-law correlating equations	
r_2/r_1	Inner wall	Outer wall	Inner wall	Outer wall
2·09	unwetted	unwetted	$u_1^+ = 6·62 + 2·20 \ln y_1^+$	$u_2^+ = 3·23 + 2·70 \ln y_2^+$
2·78	unwetted	unwetted	$u_1^+ = 10·90 + 1·77 \ln y_1^+$	$u_2^+ = 6·20 + 2·31 \ln y_2^+$
4·00	unwetted	unwetted	*	$u_2^+ = 4·12 + 2·57 \ln y_2^+$
2·09	wetted	unwetted	$u_1^+ = 2·63 + 1·94 \ln y_1^+$	$u_2^+ = 2·14 + 2·85 \ln y_2^+$
4·00	wetted	unwetted	*	$u_2^+ = 1·26 + 2·85 \ln y_2^+$
4·00	wetted	wetted	*	$u_2^+ = 2·54 + 2·77 \ln y_2^+$

* Results did not obey the logarithmic law (see Fig. 8).

Table 4. Summary of results on the matter of Reynolds-number dependency of the u^+ *— vs. —* $\ln y^+$ *data points*

r_2/r_1	Inner wall	Outer wall	Inner portion	Outer portion
2·09	unwetted	unwetted	a	a
2·78	unwetted	unwetted	b	a
4·00	unwetted	unwetted	b	d
2·09	wetted	unwetted	a	a
4·00	wetted	unwetted	b	b*
4·00	wetted	wetted	c*	d

[a] No segregation of data points according to *Re*.
[b] Very slight tendency for high-*Re* points to fall above "average."
[c] Very slight tendency for high-*Re* points to fall below "average."
[d] Slight tendency for high-*Re* points to fall below "average."
* Exception to general pattern.

If the constants and coefficients of those five equations are averaged, one gets the equation

$$u_2^+ = 3{\cdot}20 + 2{\cdot}56 \ln y_2^+, \qquad (2)$$

which is significantly different from the equation

$$u_2^+ = 1{\cdot}26 + 2{\cdot}85 \ln y_2^+, \qquad (3)$$

which is the equation of the line indicated by the combined data points. Thus, at the larger values of r_2/r_1, where there is a noticeable Reynolds dependence, a single straight line drawn through the data points for a range of Reynolds numbers is not a satisfactory way to represent the data. It is noteworthy that the slopes of the u_2^+ vs. $\ln y_2^+$ lines for the individual Reynolds numbers are uniformly significantly less than the slope of the line through the combined data points for all the five Reynolds numbers, as seen by comparing the coefficients of equations (2) and (3). It is also noteworthy that the coefficients in the equations in Table 5 are, on the average, very close to the coefficient of 2·5 in the well known Nikuradse [9] equation for pipes [see equation (4)].

Table 5. Correlating equations obtained for different Reynolds numbers for case of $r_2/r_1 = 4{\cdot}0$*, inner wall wetted, outer wall unwetted, and outer portions of annulus*

Reynolds number	Correlating equations
105400	$u_2^+ = 3{\cdot}21 + 2{\cdot}40 \ln y_2^+$
163200	$u_2^+ = 3{\cdot}23 + 2{\cdot}61 \ln y_2^+$
227500	$u_2^+ = 3{\cdot}04 + 2{\cdot}56 \ln y_2^+$
337000	$u_2^+ = 3{\cdot}05 + 2{\cdot}62 \ln y_2^+$
468100	$u_2^+ = 3{\cdot}39 + 2{\cdot}61 \ln y_2^+$

There is one respect in which the results of the present study differ from those of Quarmby. He reported that the average slope of the curves increases with increase in Reynolds number in the inner portion of an annulus and decreases in the outer portion. On the other hand, in this study, the u^+ vs. $\ln y^+$ lines (or curves) for the different Reynolds numbers were essentially parallel, other conditions remaining the same.

4.3.2 *Effect of radius ratio* (r_2/r_1). Figure 6 presents the results obtained on all three radius ratios, for the *outer* portions of the annuli, and

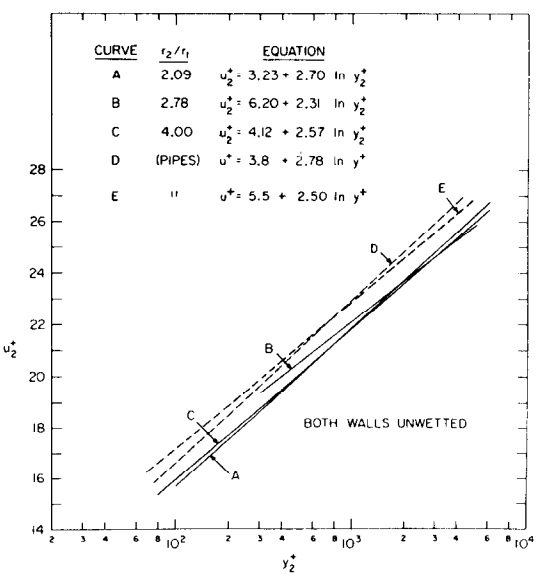

FIG. 6. Nondimensional plot of present velocity-distribution results in *outer* portions of annuli, showing that there is no significant effect of radius ratio.

for the condition where both walls were unwetted. As mentioned earlier, the general fluid-dynamic behavior for this condition was found to come closest to that for ordinary fluids. It is seen that the results are in quite good agreement and do not show a radius ratio effect, at least in the range $2{\cdot}09 \leqslant r_2/r_1 \leqslant 4{\cdot}00$. Actually, the larger the radius ratio, the greater should be the tendency for the fluid-dynamic behavior in the outer portions of concentric annuli to conform to that in circular tubes. The line for $r_2/r_1 = 2{\cdot}78$ shows a relatively low slope compared with the other lines in the figure, but the results for that particular radius ratio generally seemed to be significantly out-of-line compared with those for the other two ratios.

The two dashed lines in Fig. 6 are for the two well known equations for pipe flow. The Nikuradse [9] equation

$$u^+ = 5{\cdot}5 + 2{\cdot}5 \ln y^+ \tag{4}$$

is generally considered to work best over the whole range $50 \leqslant y^+ \leqslant 10^5$, while the Deissler [10] equation

$$u^+ = 3{\cdot}8 + 2{\cdot}78 \ln y^+ \tag{5}$$

is generally considered to work best over the range $50 \leqslant y^+ \leqslant 5000$, which is the range covered in the present study. If a single line were drawn through the data points for all three radius ratios, it would give

$$u_2^+ = 4{\cdot}28 + 2{\cdot}55 \ln y_2^+. \tag{6}$$

As seen in the figure, equations (4) and (5) are actually not greatly different in the y_2^+ range covered, and both give u^+ values that are about 5 per cent greater than the u_2^+ values obtained here.

These results are in general agreement with those obtained by Brighton and Jones [7] and by Quarmby [8] on air. Brighton and Jones found their u_2^+ vs. $\ln y_2^+$ results for $r_2/r_1 = 1{\cdot}78$ to agree with equation (4) and their results for $r_2/r_1 = 16{\cdot}0$ fell about 5 per cent below that. Quarmby found his u_2^+ vs. $\ln y_2^+$ results for

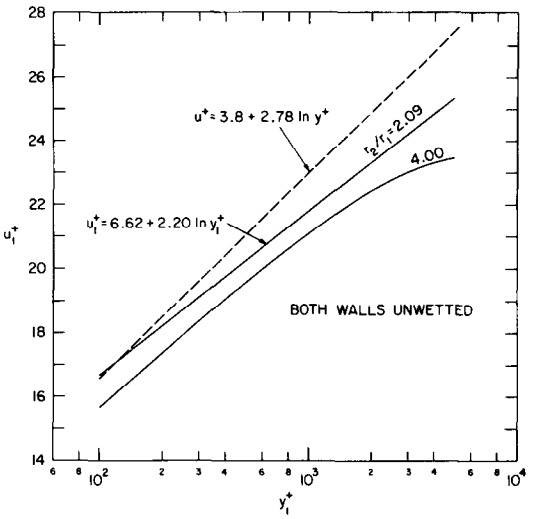

FIG. 7. Nondimensional plot of velocity distribution results in *inner* portions of concentric annuli, showing that there is an appreciable dependency on radius ratio.

radius ratios of 2·88, 5·62 and 9·37 to fall on a single line whose equation was

$$u_2^+ = 4{\cdot}6 + 2{\cdot}62 \ln y_2^+ \tag{7}$$

which agrees rather well with equation (6), obtained in the present study.

Figure 7 shows results obtained in the present study for the *inner* portions of annuli having r_2/r_1 ratios of 2·09 and 4·00. The results for the 2·78 ratio are not shown, because as explained earlier, it is felt they are a little irregular. The 2·78 data points gave a straight line that fell between those for 2·09 and 4·00, but had a generally lower slope (1.77).

The "inner-portion" results are quite different from those for the outer portion, on two counts: first, the logarithmic law does not hold at the higher r_2/r_1 ratios, and secondly, there is a rather strong radius-ratio dependence. The higher the radius ratio, the lower will be u_1^+, other things being equal. These results are consistent with those obtained by Brighton and Jones and by Quarmby on air.

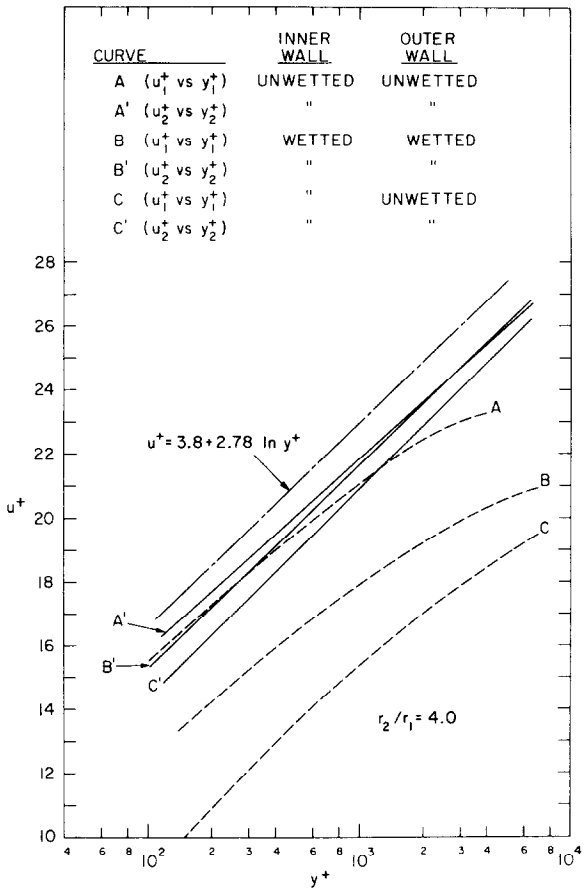

FIG. 8. Nondimensional plot of velocity distributions in both *inner* and *outer* portions of a concentric annulus. These results show a large effect of wetting, particularly in the inner portions.

4.3.3 *Effect of wetting.* As we saw earlier, the shape of the velocity profile curves depended on whether one wall was wetted, both were wetted, or both were unwetted. And, of course, this is reflected in the u^+ vs. $\ln y^+$ curves. Figure 8 dramatically illustrates this. The effect of wetting is seen to be much greater in the inner portion than in the outer portion. It is interesting to note that the fluid-dynamic behavior for the case of both walls unwetted came the closest to that generally accepted for ordinary fluids, and that for the case of the inner wall wetted and the outer wall unwetted came the farthest from that for ordinary fluids.

Figure 9 shows some results, illustrating the effect of radius ratio, for the case of a wetted inner wall and an unwetted outer wall. In this case, it will be noticed that there is a strong effect of r_2/r_1 on the lines (or curves) for the outer portion as well as on those for the inner portion, which is quite different for the "unwetted" results shown in Fig. 6.

The results obtained in this study show without doubt that wetting (compared to nonwetting) has a big influence on the shape of the velocity profile. To the present authors' knowledge, this is the first study where the effect of wetting on the velocity profile has been studied in liquid–metal flow, in any shape of channel. It appears to be a fruitful area for further investigation.

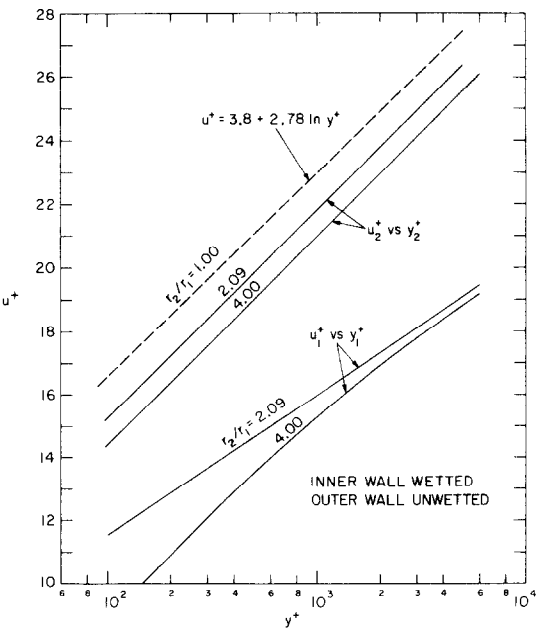

FIG. 9. Nondimensional plot of velocity distributions in both *inner* and *outer* portions of concentric annuli, illustrating an appreciable effect of radius ratio when the inner wall is wetted and the outer wall in unwetted. The dashed line ($r_2/r_1 = 1{\cdot}00$) represents Deissler's equation for pipes, which also holds for parallel plates. It is merely shown for reference and is not intended to represent the situation of one plate wetted and the other unwetted.

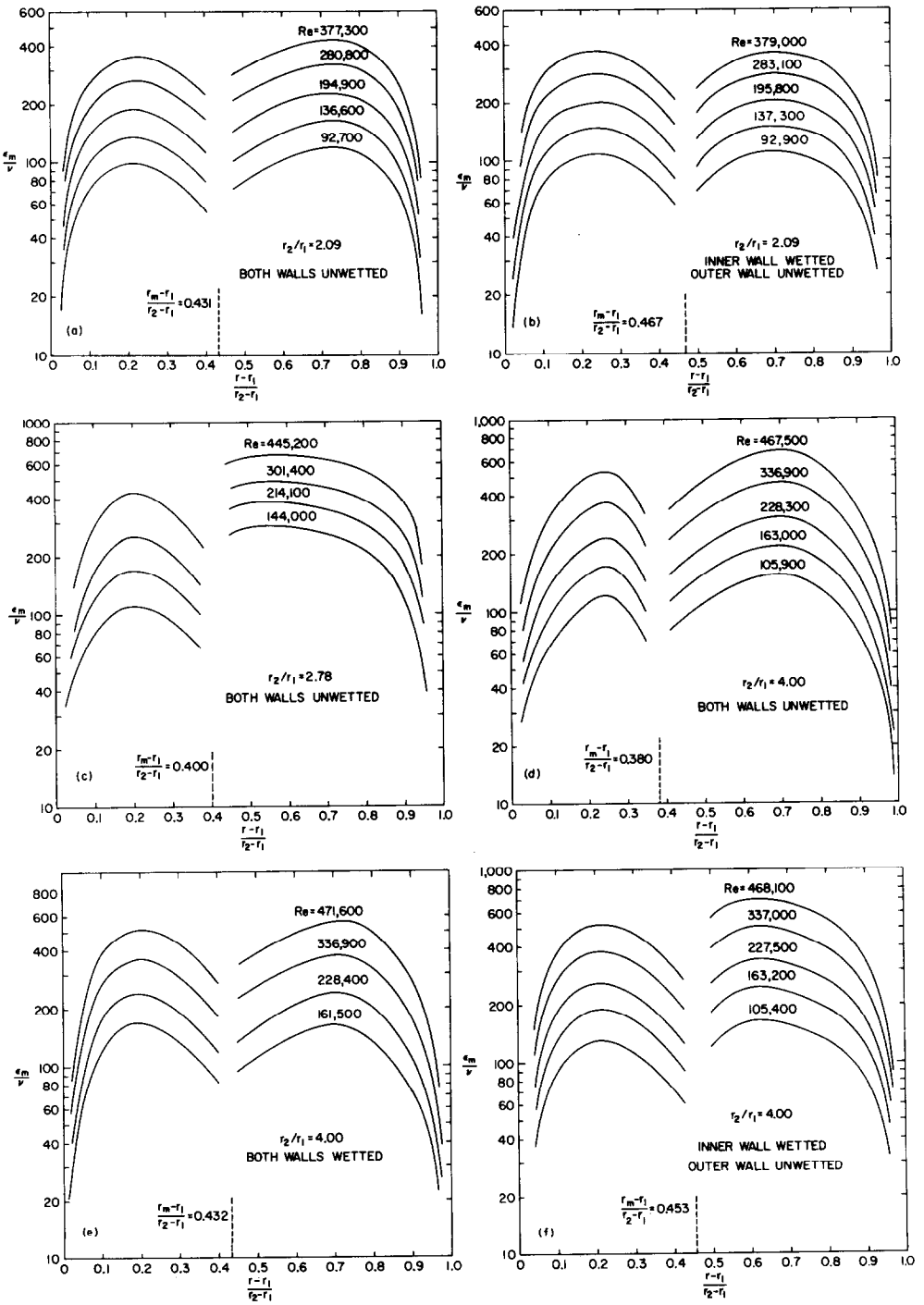

FIG. 10. Results of present study showing the radial variation of ε_M/ν, as affected by wetting conditions, by change in Reynolds number, and by change in radius ratio.

4.4 *Eddy diffusivity*

The eddy diffusivity of momentum transfer, ε_M, defined by the equation

$$\tau g_c/\rho = (\nu + \varepsilon_M)\frac{dv}{dr} \tag{8}$$

was calculated from the original data as follows.

1. The shear stress τ_1 for the inner portion of an annulus was calculated by means of the equation

$$\tau_1 = -(\Delta p/\Delta L)\frac{(r_m^2 - r^2)}{2r} \tag{9}$$

and for the outer portion, by

$$\tau_2 = -(\Delta p/\Delta L)\frac{(r^2 - r_m^2)}{2r} \tag{10}$$

where $\Delta p/\Delta L$ is the pressure gradient that was actually measured in the test section.

2. The slopes, dv/dr, of the velocity profile curve were determined graphically, by drawing tangents to the velocity profile curve. The slopes thus obtained were determined to have an average error of no more than $\pm 1{\cdot}5$ per cent. In fact, the calculated slopes were most probably more accurate than the shapes of the curves of which they were taken. The curves were the final, smoothed, normalized curves described in Section 4.1.
3. In a given case, values of ε_M were calculated [by means of either equation (9) or (10)] for many radial distances between r_1 and r_2 and plotted on an ε_M/ν vs. $(r - r_1)/(r_2 - r_1)$ plot, with Reynolds number as the parameter. A cross plot of the results was then made on an ε_M/ν vs. Re plane, and smooth curves were drawn through the points. The final results were then replotted on an ε_M/ν vs. $(r - r_1)/(r_2 - r_1)$ plane, with Reynolds number as parameter.

The results are summarized in Figs. 10a–10f. Those in Fig. 10a are for the case of *both walls unwetted*, while those in 10b are for the case of *inner wall wetted and outer wall unwetted*. The curves in Fig. 10a look quite normal and very similar to those for turbulent flow of ordinary fluids concentric annuli. The regions close to the walls and in the near vicinity of the radius of maximum velocity presented obvious calculational difficulties. That is why the curves do not extend into those regions. The curves, however, strongly suggest that they should possess minima at the radii of maximum velocity.

By comparing the curves in Fig. 10a and 10b, the effect of wetting the inner wall is seen. As explained in Section 4.2, wetting of the inner wall causes the radius of maximum velocity to move outward. This increases τ_1 in the inner portion of the annulus and decreases dv/dr to the left of $[\varepsilon_{M1}]_{max}$ and increases dv/dr to the right of $[\varepsilon_{M1}]_{max}$ and has the opposite effect in the outer portion. The result is that wetting the inner wall raises the ε_M/ν curves in the inner portion and lowers them in the outer portion. The ratio $[\varepsilon_{M1}]_{max}/[\varepsilon_{M2}]_{max}$ in Fig. 10a is about 0·83 for all Reynolds numbers, whereas in Fig. 10b it is about 1·00. It is also pointed out that the radial locations of $[\varepsilon_{M1}]_{max}$ and $[\varepsilon_{M2}]_{max}$ are independent of Reynolds number, and finally that the effect of Reynolds number on ε_M/ν is the same in both portions of the annulus, in both Figs. 10a and 10b. Actually, ε_M/ν was found to be proportional to $(Re + 15000)^{0{\cdot}96}$.

Figure 10c presents the results for the case of $r_2/r_1 = 2{\cdot}78$, with both walls unwetted. As stated before, the data for this case are consistently out of line, and the irregularity shows up here too. The curves for the inner portion appear satisfactory, but those for the outer portion are both too high and have the wrong shape.

The results for the radius ratio of 4·00 are given in Figs. 10d–10f. Figure 10d presents the results for the situation where both the inner and outer walls are unwetted, and everything looks normal. Figure 10e presents the results for the case of both walls wetted. Comparing these with those in Fig. 10d, it is seen that the two sets of curves are quite consistent. Wetting both walls has more of an effect on the inner portion of the annulus than on the outer

portion, pushes r_m to the right, and tends to raise $[\varepsilon_{M1}]_{max}$ and lower $[\varepsilon_{M2}]_{max}$.

Figure 10f presents the results for the situation where the inner wall was wetted and the outer wall was unwetted. There, the relative heights of the "inner-portion" curves are the same as they are in Fig. 10d, which is not what one might expect. Wetting the inner wall pushes the radius of maximum velocity outward, and that increases τ_1 and decreases τ_2, thereby tending to equalize the heights of the inner-portion and outer-portion eddy diffusivity curves. In the inner portion, pushing the radius of maximum velocity outward tends to decrease dv/dr in the region inside the radius of $[\varepsilon_{M1}]_{max}$, thereby tending to increase ε_{M1} in that region. In the radial region between $[\varepsilon_{M1}]_{max}$ and v_{max}, the reverse is true. This causes the radius of $[\varepsilon_{M1}]_{max}$ to move to the left. The curves in Figs. 10d and 10f bear this out. Actually, wetting only the inner wall moved r_m to the right 19 per cent and moved the radius of $[\varepsilon_{M1}]_{max}$ to the left 16 per cent. A similar line of reasoning can be followed to explain why wetting the inner wall should move $[\varepsilon_{M2}]_{max}$ to the left. In the present situation, it was shifted about 10 per cent to the left.

The relative heights of the ε_M profiles in the inner and outer portions of an annulus depend, of course, on the magnitude of the radius ratio, other things being equal. In this connection, it is interesting to examine the relation between $[\varepsilon_{M1}]_{max}/[\varepsilon_{M2}]_{max}$ and radius ratio. Recent experimental results are compared in Fig. 11, along with those obtained in the present study for the situation where both walls were unwetted. The dashed curve is merely a best-by-eye curve drawn through the results; it has no theoretical basis, except of course at its two limits. There is a surprising degree of agreement between the results of the four separate investigations. Those of Brighton [11] are the most out of line, which tends to cast some uncertainty on the accuracy of his ε_M/ν profiles, including those given in [7]. Only the both-walls-unwetted results of the present study are shown in Fig. 11, because, as pointed out earlier, they seemed to agree quite

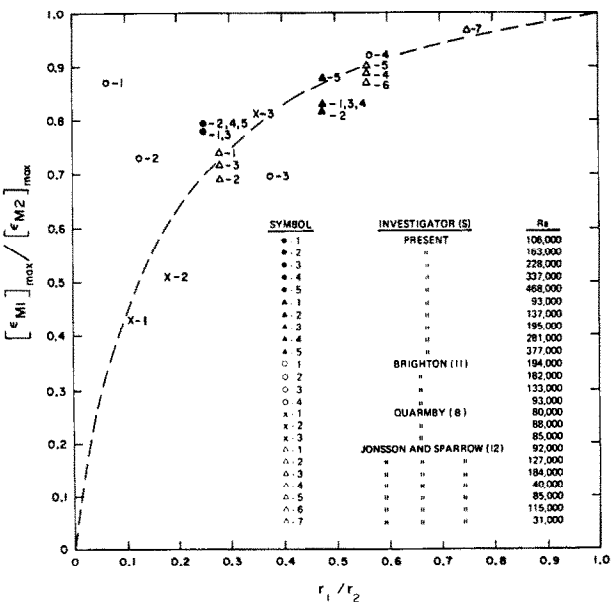

FIG. 11. Dependence of the ratio $[\varepsilon_{M1}]_{max}/[\varepsilon_{M2}]_{max}$ on the radius ratio. Comparison of present "unwetted" results with those of previous investigators on air.

well in all respects with those previously reported on ordinary fluids.

Finally, the results of the present study, and those of the other studies shown in Fig. 11, clearly demonstrate that the ratio $[\varepsilon_{M1}]_{max}/[\varepsilon_{M2}]_{max}$ is independent of Reynolds number.

4.4.1 *Correlating* ε_M. The eddy diffusivity of momentum transfer is a function of r_2/r_1, Reynolds number, kinematic viscosity, and wetting conditions. Attempts have been made to correlate ε_M for fully developed flow in concentric annuli, but owing to the complexity of the problem, they have been more or less empirical in nature. Although these correlations are approximate at best, it was not the purpose of the present study to develop an improved correlation. That would require many more experimental results, obtained under conditions where the various independent variables were systematically varied over wide ranges. However, the correlations of Kays and Leung [6] and Eifler [13] were tested against the present results.

The Kays–Leung correlation for the inner portion is

$$\varepsilon_{M1}/\nu = \frac{(1-\bar{s})\,r_2^+}{\alpha}(1-\eta_1^2)(1+2\eta_1^2) \times [1 + 0{\cdot}6\sqrt{(r_1/r_2)}\,(\eta_1 - \eta_1^2)] \times \left\{1 - \left[1 - \frac{\bar{s} - (r_1/r_2)}{\sqrt{(\tau_{w2}/\tau_{w1})}\,(1-\bar{s})}\right]\eta_1\right\} \quad (11)$$

where

$$\alpha = 15, \quad (12)$$

$$\bar{s} = r_m/r_2, \quad (13)$$

$$r_2^+ = [r_2\sqrt{(\tau_{w2}g_c/\rho)}]/\nu, \quad (14)$$

and

$$\eta_1 = \frac{r_m - r}{r_m - r_1}; \quad (15)$$

and the Kays–Leung correlation for the outer portion is

$$\varepsilon_{M2}/\nu = \frac{(1-\bar{s})\,r_2^+}{\alpha}(1-\eta_2^2)(1+2\eta_2^2) \times [1 + 0{\cdot}6(\eta_2 - \eta_2^2]. \quad (16)$$

We change equation (12) to

$$\alpha = 50\,Re^{-0{\cdot}1} \quad (17)$$

in order to achieve a better fit to our results. The eddy diffusivity normally varies as the Reynolds number carried to a power slightly greater or less than 1, depending on the Reynolds number; and r_2^+ should vary as the 0·9 power of the Reynolds number. Thus, there is some justification for including $Re^{0{\cdot}1}$ in equation (11) and (16).

Comparison between the present results and those predicted by the modified forms in equations (11) and (16) are shown in Figs. 12a, 12c, 13a and 13c, for four typical cases. When one considers the inherent lack of precision in determining ε_M profiles, the agreement in the figures is probably not bad. The major disagreement occurs in the radial region around the radius of maximum velocity, the experimental results falling much lower than those predicted by the Kays–Leung equations. The sharp minimum in the ε_M profile in the vicinity of r_m shown by the present results is, however, in agreement with the experimental results of Kays and Leung [6], Quarmby [8], and Jonsson and Sparrow [12], on air.

The second correlation investigated—that published by Eifler [13] in 1969— is a semi-empirical equation, based to a large extent on the experimental results of Brighton [11]. The equation (written for the inner portion) is

$$\varepsilon_{M1}^+ = \frac{\beta}{2(1+t_1)}(t_1 + z_1^2)(1 - z_1^2)\,f(z_1), \quad (18)$$

where β is theoretically the reciprocal of the

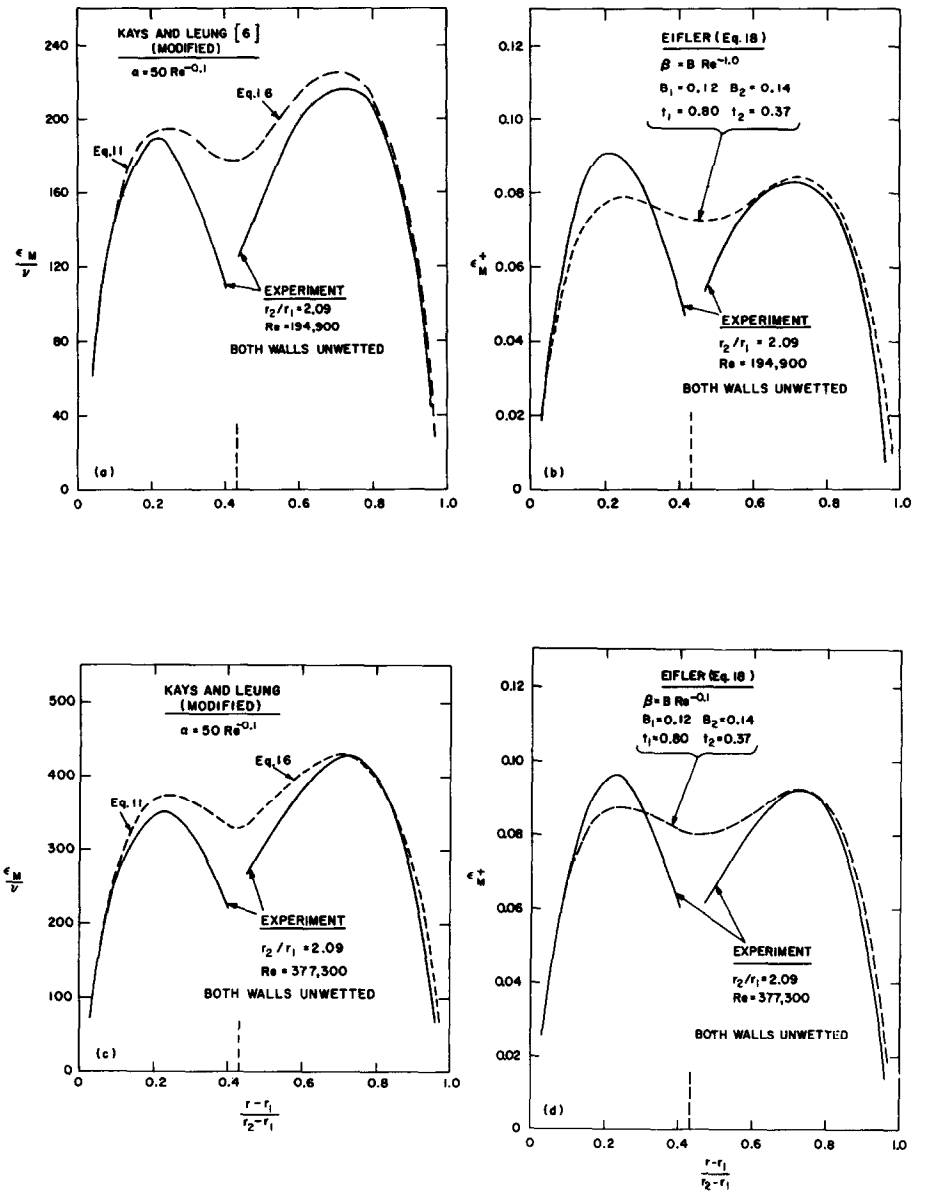

FIG. 12. Comparison of present ε_M results with those predicted by the modified correlations of Kays and Leung [6] and of Eifler [13]. The experimental results are for the case of $r_2/r_1 = 2{\cdot}09$ with both walls unwetted. The Kays–Leung correlation was modified by substituting $50Re^{-0{\cdot}1}$ in place of 15 for α; and the Eifler correlation was modified by substituting $BRe^{0{\cdot}1}$ for β, adjusting the constants B_1, B_2, t_1 and t_2 to give the best agreement with the experimental curves.

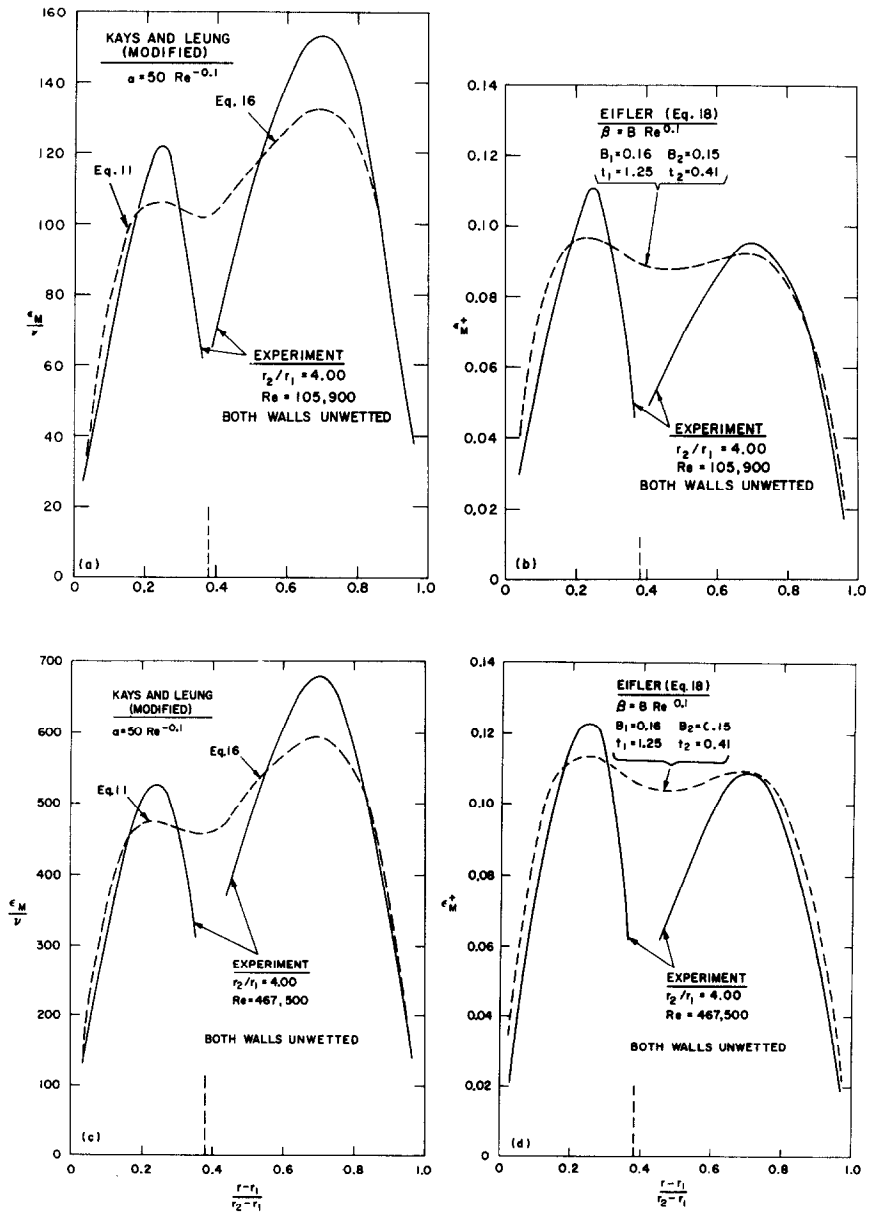

FIG. 13. Comparison of present ε_M results with those predicted by the modified correlations of Kays and Leung [6] and of Eifler [13]. The experimental results are for the case of $r_2/r_1 = 4{\cdot}00$ with both walls unwetted. The Kays–Leung correlation was modified by substituting $50Re^{-0{\cdot}1}$ in place of 15 for α; and the Eifler correlation was modified by substituting $BRe^{0{\cdot}1}$ for β, adjusting the constants B_1, B_2, t_1 and t_2 to give the best agreement with the experimental curves.

coefficient (before $\ln y^+$) in the standard law-of-the-wall velocity-distribution equation [e.g. equation (4)], and where

$$\varepsilon_{M1}^+ = \frac{\varepsilon_{M1}}{(r_m - r_1)\sqrt{(\tau_{w1} g_c)/\rho}}, \tag{19}$$

$$f(z_1) = \frac{2\left(\frac{r_m}{r_1}\right) - z_1\left(\frac{r_m}{r_1} - 1\right)}{\left(\frac{r_m}{r_1} + 1\right)\left[\frac{r_m}{r_1} - z_1\left(\frac{r_m}{r_1} - 1\right)\right]}, \tag{20}$$

and

$$z_1 = \frac{r_m - r}{r_m - r_1}. \tag{21}$$

The equation for the outer portion is the same as equation (18), except the subscript 1 on ε_M^+, ε_M, τ_w, t, z and r is changed to 2.

As they did in the Kays–Leung correlation, the present authors made certain changes in equation (18) to improve its fit to their (mercury) results (for both walls unwetted). Accordingly, β was replaced by $BRe^{0.1}$, where B is an empirical constant. Also, in certain cases, the values of t_1 and t_2 that were used were somewhat different from those recommended by Eifler, which were based on Brighton's data. An obvious requirement is that the values of B_1, B_2, t_1 and t_2 be such that the ε_{M1} and ε_{M2} profiles merge.

Figures 12b, 12d, 13b and 13d present comparisons between observed results and those predicted by Eifler's correlation. The agreements are not as good as those in Figs. 12a and 12c; while in Figs. 13b and 13d the agreements are about as good as they are in Figs. 13a and 13c. The Kays–Leung correlation shows better agreement near the walls, the Eifler correlation shows better agreement in the region of $[\varepsilon_{M2}]_{max}$, and both give ε_M values in the region of r_m that are considerably higher than those obtained experimentally.

The somewhat better agreement between the experimental curves and those given by the Kays–Leung correlation, than between the experimental curves and those given by the Eifler correlation, is noteworthy, because the former correlation has only one adjustable constant, while the latter has four (two each for the inner and outer portions).

The experimental results of Brighton [11], and the correlation of Eifler [13], which is based on Brighton's results, show $[\varepsilon_M]_{min}$ occurring at radial locations somewhat greater than r_m. However, the present results very strongly indicate, and the Kays–Leung correlation predicts, that $[\varepsilon_M]_{min}$ should occur at r_m. This was also observed by Jonsson and Sparrow [12] in their experiments with air.

REFERENCES

1. B. G. Nimmo, O. E. Dwyer and P. J. Hlavac, Radial temperature distribution and eddy diffusivity of heat transfer for turbulent flow of mercury in annuli. To be published.
2. O. E. Dwyer, P. J. Hlavac and B. G. Nimmo, Experimental study of heat transfer to mercury flowing turturbulently in concentric annuli. To be published.
3. J. L. Livesey, Design of total pressure probes for minimum interference with measured flow, *J. Aeronaut. Sci.* **21**, 641 (1954).
4. B. M. Smolskii and I. T. Elperin, The effects of surface phenomena on transfer processes in heterogeneous systems. *Int. Chem. Engng* **3**, 67–76 (1963).
5. N. F. Dokuchaev, *Sb. Issledovanie Protsessov Perenosa Tepla, Massy i Energii* (Collection of Papers on Investigation of the Processes of Heat, Mass, and Momentum Transfer), *Vsesoyuznogo Zaochnogo In-ta Pishcheroi Prom.*, Vol. 3. Moscow (1958). As referenced by [4].
6. W. M. Kays and E. Y. Leung, Heat transfer in annular passages—hydrodynamically developed turbulent flow with arbitrarily prescribed heat flux, *Int. J. Heat Mass Transfer* **6**, 537–57 (1963).
7. J. A. Brighton and J. B. Jones, Fully developed turbulent flow in annuli, *J. Basic Engng* **86**, 835–844 (1964).
8. A. Quarmby, An experimental study of turbulent flow through concentric annuli., *Int. J. Mech. Sci.* **9**, 205–21 (1967).
9. J. Nikuradse, Gesetzmaessigkeiten der turbulenten Stroemung in glatten Rohren, *VDI-Forschungsheft* **356**, 36 (1932).
10. R. G. Deissler, Investigation of turbulent flow and heat transfer in smooth tubes including the effects of variable fluid properties. *Trans. Am. Soc. Mech. Engrs* **73**, 101–107 (1951).
11. J. A. Brighton, The structure of fully developed flow in annuli, Ph.D. Thesis, Purdue University (1963).
12. V. K. Jonsson and E. M. Sparrow, Turbulent diffusivity for momentum transfer in concentric annuli, *J. Basic Engng* **88**, 550–552 (1966).
13. W. Eifler, Calculation of turbulent velocity distribution and skin friction in concentric annuli (in German), *Warme- und Stoffubertragung* **2**, 36–46 (1969).

ETUDE EXPERIMENTALE DE L'EFFET DE MOUILLAGE SUR L'ECOULEMENT TURBULENT DU MERCURE DANS UN ESPACE ANNULAIRE

Résumé– On a effectué une étude expérimentale et fondamentale de la dynamique aussi bien que des caractéristiques thermiques du mercure en écoulement turbulent établi dans un espace annulaire. Les objectifs principaux de cette étude sont tout d'abord de comparer les valeurs locales ε_H et ε_M, puis de déterminer l'effet du mouillage sur la dynamique et sur la thermique. Cet article présente uniquement les résultats relatifs à la dynamique.

Des expériences ont été faites avec le mercure soit qu'il ne mouille pas du tout, soit qu'il mouille bien les parois du canal. Les effets du mouillage sont appréciables. Lorsque les deux parois de l'anneau ne sont pas mouillées les profils de vitesse sont pratiquement identiques à ceux déjà rapportés pour les fluides ordinaires. Quand seule la paroi interne est mouillée, le rayon de vitesse maximale se déplace considérablement vers l'extérieur (vers r_2); lorsque les deux parois sont mouillées, le rayon de vitesse maximale se déplace aussi vers l'extérieur mais pas autant que dans le cas précédent. Ces différences sont marquées dans les lois de variation de u^+ en fonction de $\ln y^+$ et dans les profils ε_M.

Le mouillage est trouvé avoir une grande influence sur la loi u^+ ($\ln y^+$) pour la région intérieure de l'anneau. La diffusion de quantité de mouvement par turbulence ne s'accorde que modérément bien aux lois de Kays–Leung [6] et de Eifler [13]. On constate que le rapport des valeurs maximales de ε_M dans la région intérieure et dans la région extérieure de l'anneau est une fonction explicite du rapport des rayons et est indépendant du nombre de Reynolds.

EXPERIMENTELLE UNTERSUCHUNG ÜBER DEN EINFLUSS DER BENETZUNGSVERHÄLTNISSE BEI TURBULENTER QUECKSILBERSTRÖMUNG IN RINGROHREN

Zusammenfassung—Es wurde eine grundlegende Untersuchung über das hydrodynamische und thermische Verhalten von Quecksilber bei voll ausgebildeter turbulenter Strömung in Ringrohren angestellt. Das Hauptziel dieser Untersuchung war, vergleichbare Werte für örtliche ε_H, und ε_M-Werte zu erhalten und ferner den Einfluss der Benetzung sowohl auf das hydrodynamische Verhalten als auch auf das Wärmeübergangsverhalten zu klären. Dieser Beitrag berichtet über die hydrodynamischen Versuche.

Die Versuche wurden einmal bei völliger Nichtbenetzung der Kanalwände und einmal bei völliger Benetzung mit Quecksilber durchgeführt. Der Einfluss der Benetzung war merklich. Wurden beide Wände des Ringrohres nicht benetzt, so war das Geschwindigkeitsprofil sehr ähnlich dem, wie es bei gewöhnlichen Flüssigkeiten bekannt ist. Wenn nur die innere Wand benetzt wurde, wanderte der Radius der maximalen Geschwindigkeit von dem Ort bei Nichtbenetzung beider Wände, in Richtung auf das äussere Rohr (d.h. auf r_2 zu). Waren beide Wände benetzt, wanderte der Radius der maximalen Geschwindigkeit ebenfalls nach aussen, jedoch nicht so weit, wie im Fall, in dem nur die innere Wand benetzt wurde. Die Unterschiede im hydrodynamischen Verhalten werden in der Beziehung zwischen u^+ und $\ln y^+$ und in den ε_M-Profilen wiedergegeben.

Die Benetzungsverhältnisse haben danach einen grossen Einfluss auf die Beziehung zwischen u^+ und $\ln y^+$ im inneren Teil des Ringspalts. Der Turbulenzgrad des Impulsaustausches konnte nur einigermassen wiedergegeben werden mit der abgeänderten Form der Kays–Leung [6] und Eifler [13]-Beziehung. Es wird gezeigt, dass das Verhältnis des grössten Wertes von ε_M im inneren Teil des Ringspaltes zu dem im äusseren Teil eine explizite Funktion des Durchmesserverhältnisses und unabhängig von der Reynolds-Zahl ist.

ЭКСПЕРИМЕНТАЛЬНОЕ ИССЛЕДОВАНИЕ ВЛИЯНИЯ СМАЧИВАНИЯ НА ТУРБУЛЕНТНЫЙ ПОТОК РТУТИ В КОЛЬЦЕВОМ ЗАЗОРЕ

Аннотация—Проведено экспериментальное исследование гидродинамики и теплообмена полностью развитого турбулентного течения ртути в кольцевом канале. Основная цель исследования, во-первых, получить сравнительные данные для локальных ϵ_H и ϵ_M значений и, во-вторых, определить роль фактора смачивания в первую очередь. В статье представлены результаты по гидродинамике. Опыты проводились для двух случаев: ртуть не смачивает или очень хорошо смачивает стенки канала. Когда обе стенки канала остаются несмоченными, профили скорости подобны описанным ранее для обычных жидкостей. Когда смачивается толко внутренняя стенка, радиус максимальной скорости, сдвигается наружу (т.е. в сторону) от того положения, в котором

он находился при несмоченных стенках. В случае, когда обе стенки смачиваемы, радиус положения максимальной скорости также смещается наружу, но не так сильно, как в первом случае. Эти различия в гидродинамике отражены в зависимости u^+ от $ln\ y^+$ и сказываются на профиле ϵ_M.

Найдено, что смачивание сильно влияет на зависимость u^+ от $ln\ y^+$ для внутренней части кольцевого канала. Коэффициенты турбулентной диффузии переноса количества движения удовлетворительно коррелируются модифицированными уравнениями Кейса-Люнга [6] и Эйфлера [13] в модифицированном виде. Показано, что отношение максимального значения ϵ_M на внутреннем участке канала к максимальному значению на внешнем участке есть явная функция отношения радиусов, не зависящая от числа Рейнольдса.